# Metabolic-fluid dynamics model construction and scale-down design for an industrial penicillin chrysogenum fermentation with combined dissolved oxygen and glucose concentration dynamics

Wei, Peng; Haringa, Cees; Portela, Luis M.; Noorman, Henk J.

**DOI**
10.1016/j.ces.2023.118770

**Publication date**
2023

**Document Version**
Final published version

**Published in**
Chemical Engineering Science

Chemical Engineering Science 276 (2023) 118770

Contents lists available at ScienceDirect

Chemical Engineering Science

journal homepage: www.elsevier.com/locate/ces

# Metabolic-fluid dynamics model construction and scale-down design for an industrial *penicillin chrysogenum* fermentation with combined dissolved oxygen and glucose concentration dynamics

Peng Wei [a,b,*], Cees Haringa [c], Luis M. Portela [a], Henk J. Noorman [c,d,*]

[a] Delft University of Technology, Department of Chemical Engineering, van der Maasweg 9, 2629 HZ Delft, the Netherlands
[b] Delft University of Technology, Department of Water Management, Stevinweg 1, 2628 CN Delft, the Netherlands
[c] Delft University of Technology, Department of Biotechnology, van der Maasweg 9, 2629 HZ Delft, the Netherlands
[d] Royal DSM, Alexander Fleminglaan 1, 2613 AX Delft, the Netherlands

ARTICLE INFO

*Keywords:*
Oxygen
Glucose
CFD-CRD
Scale-down
Penicillin fermentation

ABSTRACT

This study focuses on the metabolic impacts of simultaneous glucose and oxygen concentration gradients on penicillin production in an industrial-scale fermentor, using the computational fluid dynamics-cellular reaction dynamics approach. Inclusion of oxygen-coupling considerably impacts the glucose uptake and resulting penicillin productivity. This is characterised by six metabolic regimes; lifeline data reconstructed from experimental results, recorded from the cellular perspective, indicates rapid dynamics in glucose and dissolved oxygen uptake by the microorganisms. The results are highly sensitive to variations in the oxygen-related model parameters, requiring accurate insight into the multiphase hydrodynamics and metabolic processes. Hypothetical scenarios with stronger glucose-oxygen limitations than tested experimentally were further explored. A precision scale-down (SD) simulator was designed based on the lifeline data, requiring considerable operational dynamics, with increasing system complexity and implementation difficulty. These insights may inspire further research into alternative SD configurations better suited to mimic the rapid dynamics of large-scale fermentation processes.

## 1. Introduction

The performance of microorganisms in industrial-scale fermentation processes may be affected by environmental factors, notably substrate and dissolved oxygen (DO) concentrations (Steel and Maxon 1966, Larsson et al., 1996, Manfredini et al., 1983). In large-scale fermentations, the distribution of these factors can be spatially heterogeneous, which means that throughout the process microorganisms will try to adapt to changes in their extracellular environment, acknowledging cell-to-cell differences depending on the time spent in various bioreactor zones, thus impacting overall process performance (in particular, rate and yield) (Neubauer and Junne 2010, Wang et al., 2014). The challenging task of rational process design and optimisation is to take the environmental heterogeneity into account. A detailed and high-resolution modelling framework can be a major enabler to this effort. In order to parameterise models, scale-down (SD) simulators are commonly used to probe the impact of gradients on the performance of the bioreactors, under representative industrial-scale conditions in the lab (Noorman 2011, Wang, Tang et al. 2015). An SD simulator is to be designed following 5 degrees of freedom (Noorman 2011), and typically implemented based on either a single-reactor or a multi-compartment reactor (commonly two-compartment) approach (Neubauer and Junne 2010, Wang, Chu et al. 2014). Many SD simulators have been developed for highly relevant microbial production systems, e.g., the yeast (*S. cerevisiae*) fermentation process, in which the large-scale gradients of both glucose (Sweere et al., 1988b, George, Larsson et al. 1993, George, Larsson et al. 1998, Heins, Lencastre Fernandes et al. 2015, Haringa, Deshmukh et al. 2017) and oxygen (Sweere et al., 1988a,c) have been experimentally or numerically mimicked.

Recently, a scale-down framework was developed for characterising substrate distributions in an industrial-scale (54 $m^3$) penicillin (PEN) fermentor, by developing a computational fluid dynamics-cellular reaction dynamics (CFD-CRD) model (Haringa, Tang et al. 2016, Haringa, Tang et al. 2018). Considerable substrate gradients were predicted, and characterised by specific metabolic regimes in both single phase

* Corresponding authors at: Post: P.O. Box 5046, 2600 GA Delft, The Netherlands.
*E-mail addresses:* P.Wei@tudelft.n (P. Wei), Henk.Noorman@dsm.com (H.J. Noorman).

https://doi.org/10.1016/j.ces.2023.118770
Received 3 February 2023; Received in revised form 9 April 2023; Accepted 17 April 2023
Available online 23 April 2023

**Nomenclature**

| | |
|---|---|
| $a$ | Volume specific gas bubble area, $m^2/m^3$ |
| $c$ | Stirrer blade height coefficient, - |
| $C_s$, $C_o$ | Concentrations of glucose and DO, respectively, mol/L |
| $C_x$ | Biomass concentration, g/L |
| $c^*$ | Oxygen solubility, $mol/m^3$ |
| $D_s$ | Impeller diameter, m |
| $F_{glucose}$, | $f_s$,Glucose feed rate, $mol/(m^3 \cdot s)$ |
| $K_o$ | The affinity constants for DO, mol/L |
| $K_s$ | The affinity constants for glucose, mol/L |
| $k_L$ | Oxygen mass transfer coefficient, m/h |
| $N$ | Stirring speed, $s^{-1}$ |
| $OTR$ | Oxygen transfer rate, $mol/(m^3 \cdot s)$ |
| $P_{sG}$, $P_{sU}$ | Stirring power input under gassed and ungassed conditions, W |
| $Q_G$ | Gas flow rate, $m^3/s$ |
| $q_s$, $q_o$ | Specific uptake rates of glucose and DO, respectively, $mol/(Cmol_x \cdot s)$ |
| $q_{o,max}$ | Max. specific uptake rates of DO, $mol/(Cmol_x \cdot s)$ |
| $q_{s,\ max}$ | Max. specific uptake rates of glucose, $mol/(Cmol_x \cdot s)$ |
| $R_{GU}$ | The $P_{sG}$ / $P_{sU}$ ratio, - |
| $t$ | Time, s |
| $v_G$ | Gas superficial velocity, m/s |
| $V_L$ | Liquid volume, $m^3$ |
| $Y_{os}$ | Relative DO uptake rate (to glucose uptake), -. |
| $\rho_L$ | Liquid density, $kg/m^3$ |
| $\tau_{95}$ | 95% mixing time, s |

*Abbreviations*

| | |
|---|---|
| CFD | Computational fluid dynamics |
| CRD | Cellular reaction dynamics |
| DO | Dissolved oxygen |
| PEN | Penicillin |
| QUICK | Quadratic interpolation for convective kinetics |
| SD | Scale-down |

(Haringa, Tang et al. 2016), and Eulerian-Eulerian two-phase (Haringa, Tang et al. 2018) systems. The Euler-Lagrange method has been used to assess potential environmental changes experienced by individual microorganisms (Lapin et al., 2004, 2006). The obtained lifeline data revealed rapid fluctuations (in the order of seconds) in the substrate uptake rate of the microorganisms (Haringa, Tang et al. 2016, Haringa, Tang et al. 2018). These extracellular substrate fluctuations were further integrated into the intracellular metabolism characterised by a 9-pool model (Tang et al., 2017), to investigate the metabolic response of *P. chrysogenum* for PEN production (Haringa, Tang et al. 2018). This modelling effort was supported by experimental SD studies, used to develop the metabolic model (de Jonge et al., 2011, Tang et al., 2017), and to compare performance in different SD simulators (Wang et al., 2018). In these SD studies, the industrial-scale substrate gradients were imitated by applying an intermittent substrate feed in a single-reactor simulator (de Jonge et al., 2011, Wang et al., 2018), and by feeding in one compartment of a two-compartment simulator (Wang et al., 2018), which both led to considerable reduction of the PEN productivity. However, the applied feed time scales (typically 30 s in a cycle of 360 s) seem too large to replicate the aforementioned rapid fluctuations predicted by the industrial-scale CFD model (Haringa, Tang et al. 2016, Haringa, Tang et al. 2018). These fluctuations, characterised by specified regime-transition patterns, were well represented using fluctuating pulse feed in a numerical SD simulator (Haringa, Tang et al. 2018). Although the predictions matched industrial-scale data reasonably, translating the proposed SD design to a practical setup brings about challenges, and the design has not yet been realised.

Several studies have reported that changes in the DO concentration have an important effect on the PEN production process (Vardar and Lilly 1982, Larsson and Enfors 1985, Larsson and Enfors 1988, Henriksen et al., 1997, McIntyre et al., 1999). The PEN production can be considerably inhibited, or even (reversibly/irreversibly) lost when the DO concentration was below specific thresholds (Vardar and Lilly 1982, Larsson and Enfors 1988, Henriksen et al., 1997), or under DO starvation conditions (Larsson and Enfors 1985, McIntyre et al., 1999). To simplify the model, oxygen was assumed to be non-limiting in the previous modelling work (Haringa, Tang et al. 2016, Haringa, Tang et al. 2018), supported by (unpublished) DO observations in the industrial fermentation under consideration. Similarly, the potential limitations or extracellular fluctuations of oxygen have not been addressed in the relevant numerical SD studies. Still, local DO limitations can affect bioprocesses, and further model development needs to consider the potential simultaneous impact of oxygen gradients and substrate gradients.

This study focuses on characterising the oxygen gradients by integrating oxygen transfer and depletion processes in the CFD simulation of an industrial-scale *P. chrysogenum* fermentor. The aim is to further develop the industrial-scale CFD-CRD model framework by investigating the impact of the oxygen gradients on coupled substrate uptake and PEN production, including some hypothetical scenarios with severe substrate-oxygen limitations, and to propose an SD simulator design representative to the industrial-scale system, while keeping realizability of the experimental setup in mind.

## 2. Model setup

### 2.1. Industrial-scale modelling

The CFD model was developed based on an industrial-scale fermentor for PEN production, similar to prior work (Haringa, Tang et al. 2016, Haringa, Tang et al. 2018), with an effective volume of 54 $m^3$ and two Rushton impellers for stirring (stirring speed 1.63 $s^{-1}$). Aeration was applied in the model with a superficial gas velocity of 0.05 m/s measured under standard temperature and pressure conditions. The Realizable k-ε model (Shih et al., 1995) with the dispersed turbulence multiphase model was used for turbulence simulation, and the Sliding Mesh model was used for modelling the agitators. The Eulerian-Eulerian model was applied for the aerated flows. In the current approach, the liquid phase properties were assumed similar as water, considering the challenge to integrate non-Newtonian broth rheology in the model (Haringa, Tang et al. 2018). The ideal gas law and a single-bubble size (6.4 mm) assumption were applied for the gas phase. The Grace model (Clift et al., 1978) was used for solving the drag force between the two phases, with the surface tension set to 0.073 N/m. Other interphase forces were not considered, similar to previous work (Gunyol et al., 2009, Khopkar et al., 2003, Haringa, Deshmukh et al. 2017, Haringa, Tang et al. 2018). The 3rd order discretisation scheme Quadratic interpolation for convective kinetics (QUICK) (Leonard and Mokhtari 1990) was applied for the momentum, volume fraction, and turbulence equations. Oxygen transfer between the two phases was simulated based on a hybrid mass transfer assumption. It was assumed that oxygen transport into the liquid phase is dominated by penetration in low-turbulence regions, and by surface renewal due to turbulent eddies in high-turbulence regions. Consequently, the oxygen mass transfer coefficient $k_L$ was first calculated both by the Higbie penetration model (Higbie 1935), and the Lamont-Scott Eddy-cell model (Lamont and Scott 1970); then the larger value was used to determine the local mass transfer coefficient. As in prior work (Haringa, Tang et al. 2016,

Haringa, Tang et al. 2018), the substrate (glucose) feed rate was set to 1.23 g/(m$^3$ liquid·s); the biomass concentration (55 g/L) and liquid volume were assumed to be constant; biomass growth and volume changes were considered negligible over the simulation timespan (order of minutes) in this study.

In the liquid phase, glucose and oxygen consumption was considered using a coupled assumption, which was characterised by two models. First, the Tsao & Hanson model (Tsao and Hanson 1975), in which the glucose and oxygen uptake rates were calculated as

$$q_s = q_{s,max} \bullet \frac{C_s}{C_s + K_s} \bullet \frac{C_o}{C_o + K_o} \tag{1}$$

$$q_o = q_{o,max} \bullet \frac{C_o}{C_o + K_o} \bullet \frac{C_s}{C_s + K_s} \tag{2}$$

where $q_s$ and $q_o$ denote specific uptake rates of glucose and DO, respectively; $q_{s,\ \max}$ and $q_{o,\max}$ the maximum biomass specific uptake rates of glucose and DO, respectively; $K_s$ and $K_o$ the affinity constants for glucose and DO, respectively; $C_s$ and $C_o$ local concentrations of glucose and DO, respectively. The second approach used in this study was the Roels model (Roels 1983), previously applied for the substrate-oxygen coupled consumption in other studies (Kuschel and Takors 2020, Hajian et al., 2020). The coupled metabolic kinetics were estimated by the limiting biomass growth rate between glucose and DO

$$\mu = min(\mu_s, \mu_o) \tag{3}$$

where $\mu$ the specific biomass growth rate; $\mu_s$,$\mu_o$ biomass growth rates of glucose and DO, respectively, calculated by the Herbert-Pirt correlations.

$$\begin{cases} \mu_s = \frac{1}{\alpha_s}\left(q_s - \beta_s \bullet q_P - \gamma_s \bullet q_{byp} - m_s\right) \\ \mu_o = \frac{1}{\alpha_o}\left(q_o - \beta_o \bullet q_P - \gamma_o \bullet q_{byp} - m_o\right) \end{cases} \tag{4}$$

where $m$ denotes the maintenance rate; $\alpha$, $\beta$, $\gamma$ the coefficients of biomass growth rate, PEN production rate, and byproduct formation rate, respectively. The subscripts $s$ and $o$ denote glucose and DO, respectively. The correlation with glucose repression of the PEN gene cluster (Douma et al., 2010) was also considered to calculate the PEN production rate. All oxygen-related parameters in the Tsao & Hanson model and the Roels model were taken from (Janoska et al., 2022). Additionally, a scenario with unlimited oxygen availability was simulated for reference.

An Euler-Lagrange model was applied for tracking a large number of lifelines representing the microorganism trajectories. The microorganisms were assumed as massless particles in the liquid phase. The discrete random walk model was used for the turbulent dispersion effect on the particle's motion. In each case, 20 000 particles were tracked for a flow time of 900 s (over 10 times of the simulated 95% mixing time ($t_{95}$) of the bioreactor) and the data sampling time step size was 0.03 s, to obtain lifelines with sufficient statistical meaning and accuracy (Haringa et al., 2017b). Fourier analysis on the obtained lifeline data was carried out first. A smooth spectrum, having a stabilised trend after 3 times of $t_{95}$, was observed without any frequency standing out in particular (data not shown). The results agreed with the previous work (Haringa, Tang et al. 2016), so similar to their conclusion, the Fourier analysis was not used for further data analysis.

### 2.2. Scale-down simulator design

The proposed SD simulations applied the single-reactor mode with a chemostat operation (fixed reactor volume and biomass concentration). As discussed in Haringa, Tang et al. (2018}, the time scale of mixing is smaller than the oscillations of the mean glucose concentration, so any transient change in the glucose concentration caused by feed dripping in the SD simulator was neglected, and ideal mixing was assumed. Then, the glucose mass balance between feed and consumption was calculated as

$$q_s C_x + \frac{dC_s}{dt} = F_{glucose} = \begin{cases} f_s, feedON \\ 0, feedOFF \end{cases} \tag{5}$$

where $C_x$ denotes the biomass concentration, and $F_{glucose}$ the glucose feed rate. Both feast phase (constant feed rate $f_s$) and famine phase (no feed) were included. Similarly, the oxygen mass balance could also be estimated under oxygen supply ON and OFF conditions

$$q_o C_x + \frac{dC_o}{dt} = OTR = \begin{cases} k_L a(c^* - c_o), supplyON \\ 0, supplyOFF \end{cases} \tag{6}$$

where $OTR$ denotes the oxygen transfer rate, $k_L$ the oxygen mass transfer coefficient, $a$ the volume specific gas bubble area, and $c^*$ the oxygen solubility. Due to the ideal mixing assumption, constant $k_La$ and instantaneous oxygen transfer from gas phase to liquid phase without any delaying effect were assumed. The $k_La$ is correlated with the operational parameters in a gassed and stirred bioreactor with the coalescing broth scenario, in which bubble size > 2 mm was assumed (Van't Riet 1979, Noorman et al., 2018)

$$K_L a = 0.026\left(\frac{P_{sG}}{V_L}\right)^{0.4} v_G{}^{0.5} \tag{7}$$

$$\begin{cases} P_{sG} = R_{GU} P_{sU} \\ P_{sU} = 0.5 c \pi^4 \rho_L N^3 D_s{}^5 \end{cases} \tag{8}$$

where $P_{sG}$ and $P_{sU}$ denote stirring power input under gassed and ungassed conditions, respectively, $V_L$ the liquid volume, $v_G$ the gas superficial velocity, $c$ the stirrer blade height coefficient (0.21), $\rho_L$ the liquid density, $N$ the stirring speed, and $D_s$ the impeller diameter. $R_{GU}$ is the $P_{sG}$ / $P_{sU}$ ratio, which is determined by the correlations for a single-impeller stirring tank (Cui et al., 1996)

$$R_{GU} = \begin{cases} 1 - 9.9\left(\frac{Q_G N^{0.25}}{D_s{}^2}\right), \frac{Q_G N^{0.25}}{D_s{}^2} \le 0.055 \\ 0.48 - 0.62\left(\frac{Q_G N^{0.25}}{D_s{}^2}\right), \frac{Q_G N^{0.25}}{D_s{}^2} > 0.055 \end{cases} \tag{9}$$

where $Q_G$ denotes the gas flow rate.

For SD design, we focused on oxygen-coupled lifelines generated with the Tsao & Hanson model. At this stage, we do not have the experimental data to decide whether this model or the Roels model is more representative of industrial gradients, but we expect the design challenges to be similar between them. The SD simulator design was carried out in the following three variants.

(1) SD-A: The first design was based on the SD approach developed in prior work (Haringa, Tang et al. 2018), extended to replicate oxygen-related lifelines. The single-reactor mode was still assumed, with a relatively high biomass concentration (27.5 g/L) to capture the rapid fluctuations in the lifeline profiles. Each glucose feast-famine event was coupled with oxygen dynamics, and vice-versa. For glucose lifelines to characterise metabolic regimes, the randomised feed rate and time scale were determined based on correlations between the magnitude and duration of $q_s/q_{s,\max}$, which were estimated by a proposed arc-analysis method (Haringa, Tang et al. 2016) on the industrial-scale lifeline data. Similarly, the oxygen supply mode was assumed intermittent. To characterise metabolic regimes, the time scale and the lowest $C_o$ reached in each oxygen supply-off phase were determined based on the $C_o$–related correlations from the arc-analysis. The connection and switch between different glucose feed and oxygen supply conditions were determined based on the probability of involved regime-transition patterns and logical pattern sequences.

(2) SD-B: The second design originates from practically realisable

design choices based on typical established SD simulator operation, extended to mimic the predicted simultaneous glucose-oxygen gradients to a decent degree. In this SD experiment, a relatively low biomass concentration (6 g/L) was applied. The basic cycle design and glucose feed conditions were set based on the experimental setup of de Jonge, Buijs et al. (2011); the oxygen limitation was represented by applying a DO starvation mode in the oxygen supply condition, similar to some previous studies (Larsson and Enfors 1985, McIntyre et al., 1999). More details of the experimental setup are summarised in Table S1.

(3) SD-C: based on the limitations of SD-A and SD-B, a new SD simulator design was proposed to achieve a trade-off between the adequate representation of the industrial-scale data (improvement over SD-B), and an effective translation to practically realisable SD experiments (improvement over SD-A). The details are described in Section 3.2.3.

## 3. Results and discussion

### 3.1. Glucose-oxygen coupled impacts on penicillin production in the industrial-scale fermentor

#### 3.1.1. Metabolic regime definition and dependency on oxygen-coupled uptake kinetics

In the current approach, both glucose and oxygen exert control over the uptake kinetics. First, we must consider how the presence of oxygen affects the metabolic regime definition, which was proposed for non-limiting oxygen conditions (Haringa, Tang et al. 2016). The oxygen criterion was determined by the impact of DO on PEN productivity, where the PEN production rate showed a dramatic decrease when the DO concentration was below 0.05 mmol/L (Janoska et al., 2022); the observed trend being in agreement with the correlation reported by Henriksen, Nielsen et al. (1997). Based on the static regime assumption, this critical DO concentration could be used as a threshold for limiting the PEN production process, and the PEN metabolism could be classified as either DO-sufficient ($C_o > 0.05$ mmol/L), or DO-limited ($C_o \leq 0.05$ mmol/L). Combining this with the prior glucose regimes, six metabolic regimes were defined based on the thresholds for both glucose uptake capacity ($q_s/q_{s,\max}$) and DO concentration. As shown in Table 1, each regime is determined by a sub-regime of glucose (Excess, Limitation, or Starvation, as defined before (Haringa, Tang et al. 2016)), and a sub-regime of DO (Sufficient, or Limited). The regime naming is also listed in this table and used in the rest part of this paper, with + and - for DO Sufficient and DO Limited, respectively.

We applied both glucose-oxygen uptake models to the CFD simulations, and registered the regime distribution, both with the regular glucose feed rate and a more extreme scenario with the glucose feed doubled. Table 1 contains the metabolic regime distributions for the resulting four cases. In the Tsao & Hanson model (normal feed), only 3 metabolic regimes were observed in the studied bioreactor: L-, L+, and S+, with the S- regime and glucose-Excess (E + and E-) being absent. Almost 15% of the domain was predicted to operate with limited DO concentrations (L-), detrimental for PEN production. In regions of high local glucose concentration, the limiting effect of oxygen is sufficient to avoid glucose uptake saturation, leading to the absence of the excess regime. As excess glucose may lead to repression of enzyme production in the PEN pathway (Douma et al., 2010, Tang et al., 2017, Haringa, Tang et al. 2018), this may have a positive impact on PEN production. Using the Roels model, the two glucose-Excess sub-regimes: E + and E- were predicted to be present. This difference was caused by the different approach towards calculating $q_s$ between Equation (1) and Equation (4). In the Roels model, glucose uptake is not directly affected by oxygen limitation (and vice-versa), so the glucose-Excess regime ($q_s/q_{s,\max} > 0.95$) could occur when the local glucose concentration was high enough. As this change leads to a higher local glucose uptake rates, stronger glucose gradients are observed, with larger glucose Starvation regimes (S + here). In the Roels scenario the glucose level was the limiting parameter to calculate $q_s$ in most regions, and only a small fraction (4%) of the bioreactor was under oxygen-Limited conditions (E- and L-).

It should be noted that the aforementioned differences between the two models could not be further validated, since no experimental data on oxygen distributions in the studied industrial fermentor was available. Hence, comments regarding which model presents the most realistic description of the fermentation environment are out of the current scope. For design of the scale-down setup, we focus on the Tsao & Hanson model as an example; we expect the approach to be equally applicable to the data generated with the Roels model.

#### 3.1.2. Glucose-oxygen gradients and metabolic regime distributions

The oxygen coupling effect on the glucose uptake performance was assessed first. First, results from the Tsao & Hanson model are compared with a scenario with unlimited oxygen availability, where the glucose uptake capacity ($q_s/q_{s,\max}$) was still characterised by the prior definition of metabolic regimes (Haringa, Tang et al. 2016). Fig. 1A shows the metabolic regime distributions of the two scenarios from the same frozen flow field. The results of the unlimited oxygen scenario were in good agreement with previous work (Haringa, Tang et al. 2016). The fraction differences (≤10%) in the Excess, Limitation and Starvation regimes were mainly due to the flow-field changes following the inclusion of aeration in the current model, whereas the previous work (Haringa, Tang et al. 2016) considered single-phase flow. However, the oxygen-coupled scenario (the Tsao & Hanson, normal feed in Table 1) had distinct regime distributions, with no glucose-Excess regime and a considerable decrease of the glucose-Starvation regime. These changes indicated that with the proposed kinetics, the oxygen gradients had the potential to impact the overall glucose uptake and fermentation performance.

Although with reduced size, the glucose-Starvation regime still filled the lower part of the bioreactor, due to the top feed location and high affinity for glucose uptake. The situation for oxygen was reverse: the aeration inlet is located near the bottom of the bioreactor. Additionally, the top part had relatively low DO solubility resulting from the hydrostatic pressure gradients and lower oxygen partial pressure in the gas bubbles, aggravated by a high DO depletion rate coupled with the high local glucose concentration ($C_s$) according to Equation (2). Hence, the local DO concentration ($C_o$) could very well be lower than the threshold value (0.05 mmol/L), as shown in Fig. 1B. The opposite glucose and DO gradients had a similar pattern to previous work on bioreactors for

**Table 1**
Definition of glucose-oxygen coupled metabolic regimes, and the predicted fractions (%) in the studied fermentor by the two oxygen-coupling models, with a real and a hypothetical case (doubled feed rate).

| Re-defined metabolic regime | Glucose | Oxygen | Roels, normal feed | Tsao & Hanson, normal feed | Roels, double feed | Tsao & Hanson, double feed |
|---|---|---|---|---|---|---|
| E+ | Excess (E) | Sufficient (+) | 9.0 | 0 | 11.8 | 0 |
| L+ | Limitation (L) | | 18.0 | 37.7 | 23.2 | 58.2 |
| S+ | Starvation (S) | | 69.0 | 47.5 | 51.2 | 8.0 |
| E- | Excess (E) | Limited (-) | 2.7 | 0 | 12.9 | 0 |
| L- | Limitation (L) | | 1.3 | 14.8 | 0.9 | 33.8 |
| S- | Starvation (S) | | 0 | 0 | 0 | 0 |

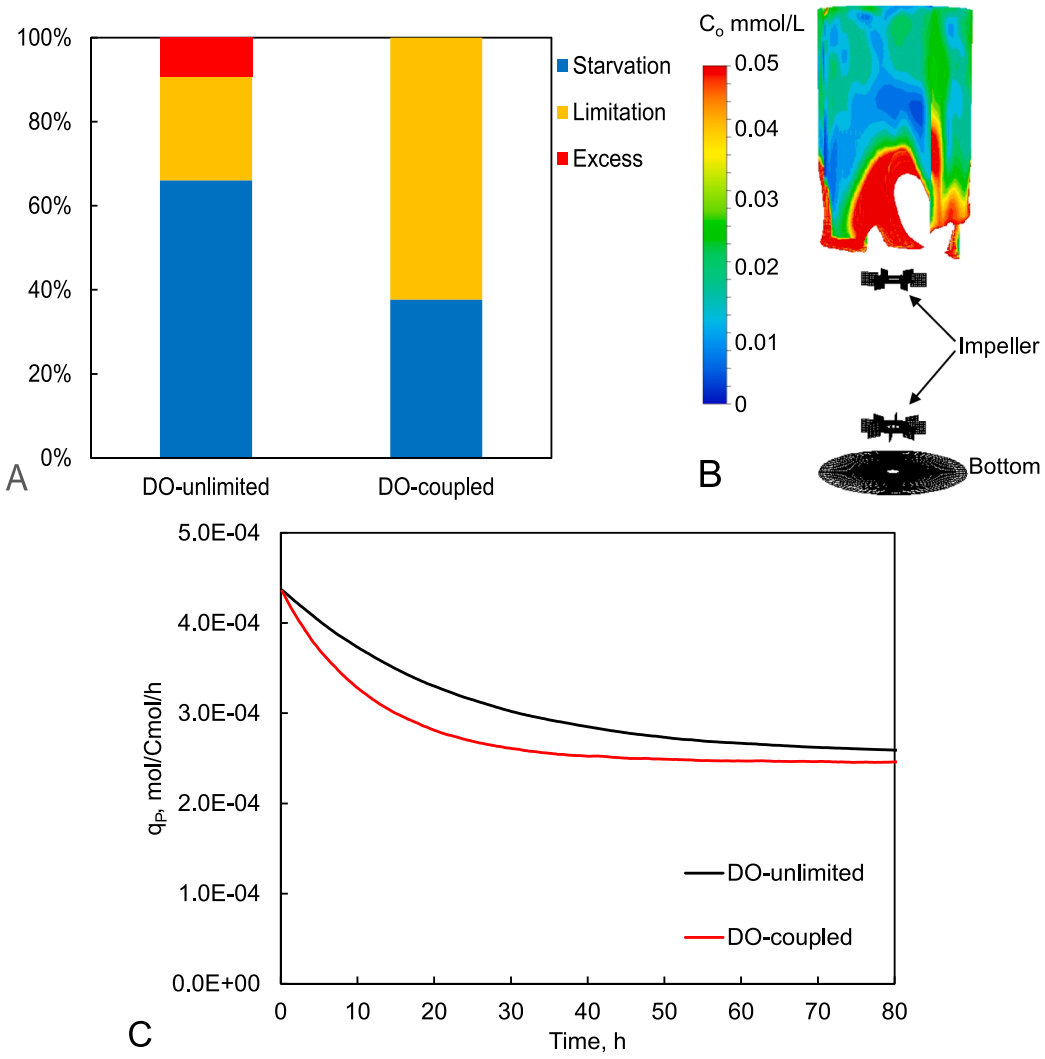


**Fig. 1.** Distributions in the studied fermentor of (A) glucose uptake regimes defined by Haringa, Tang et al. (2016), including DO-unlimited (left) and DO-coupled (right) scenarios; (B) oxygen-Limited regime ($C_o < 0.05$ mmol/L), oxygen-coupled. (C) Response of PEN production rate predicted in DO-unlimited and DO-coupled scenarios, the average of 61 elongated lifelines.

*C. glutamicum* (Kuschel and Takors 2020) and *S. cerevisiae* (Hajian et al., 2020), which also used feed on the top and aeration from the bottom. In the top part, the resulting decreased magnitude of the term $C_o/(C_o + K_o)$ led to calculate the local glucose uptake capacity lower than 0.95, and thus no Excess-regime was obtained. With the reduced DO-coupled glucose consumption in the top part, the glucose fed by the same rate could be better distributed throughout the whole bioreactor, leading to a larger fraction of the Limitation-regime, combined with a smaller fraction of the Starvation-regime.

The metabolic regime data were further integrated into the 9-pool model (Tang et al., 2017) to estimate long-term stabilised PEN production performance. It should be noted that the oxygen uptake process has not been included in the 9-pool model, hence, the model outcomes only predict the impact of the altered glucose distribution in the aerated scenario. Similar to the prior work (Haringa, Tang et al. 2018), the lifelines with a time scale of 80 h were formed by connecting the single particle's lifelines (each with a time scale of 900 s) in random order. Totally 61 elongated lifelines were obtained, and the averaged response curves are shown in Fig. 1C. It was found that the PEN production rate of the oxygen-coupled scenario dropped faster, and the stabilised rate (over 80 h fermentation time) was also lower (~5%), compared to the unlimited oxygen scenario. Although with a better overall glucose distribution (reduced size of the glucose-Starvation regime), the glucose-Excess regime, which can increase the PEN formation due to less glucose repression, was absent. Hence, if the Tsao & Hanson uptake coupling approach is combined with the 9-pool model, low DO concentrations can still negatively impact PEN production, despite the impact of oxygen not being directly accounted for by the 9-pool model. Qualitatively, the impact of low DO does follow prior experimental work in lowering PEN production (Vardar and Lilly 1982, Larsson and Enfors 1988, Henriksen et al., 1997). However, for better quantitative understanding, the impact of low DO should be directly included in a structured kinetic model, and coupled simulation results should be compared with experimental outcomes in future work.

### 3.1.3. Statistical analysis of the glucose-oxygen coupled lifelines

Regime analysis was performed on the oxygen-coupled lifeline data, yielding regime-residence time distributions and regime-transition patterns, characterising the microbial trajectories through the connected redefined metabolic regimes. Based on the applied regime distribution, six new regime-transition patterns were determined, which are summarised in Table 2 and Fig. 2A.

As shown in Table 2, the begin and end points in each regime-transition pattern were determined by specified limiting parameters from both glucose and oxygen, leading to different profile characteristics between glucose ($q_s/q_{s,\max}$) and oxygen ($C_o$) lifelines. Generally, all

**Table 2**
Determination of glucose-oxygen coupled regime-transition patterns, $q_s/q_{s,max}$ dimensionless.

| Pattern | Regime transition: from/in/to | Limiting parameters, begin point | Lifeline stays | Limiting parameters, end point |
|---|---|---|---|---|
| **1** | L+/L-/L+ | $C_o$ 0.05 mmol/L; glucose in Limitation | L- | $C_o$ 0.05 mmol/L; glucose in Limitation |
| **2** | S+/L+/S+ | DO in Sufficient; $q_s/q_{s,max}$ 0.05 | L+ | DO in Sufficient; $q_s/q_{s,max}$ 0.05 |
| **3** | S+/L+/L- | DO in Sufficient; $q_s/q_{s,max}$ 0.05 | L+ | $C_o$ 0.05 mmol/L; glucose in Limitation |
| **4** | L-/L+/L- | $C_o$ 0.05 mmol/L; glucose in Limitation | L+ | $C_o$ 0.05 mmol/L; glucose in Limitation |
| **5** | L-/L+/S+ | $C_o$ 0.05 mmol/L; glucose in Limitation | L+ | DO in Sufficient; $q_s/q_{s,max}$ 0.05 |
| **6** | L+/S+/L+ | DO in Sufficient; $q_s/q_{s,max}$ 0.05 | S+ | DO in Sufficient; $q_s/q_{s,max}$ 0.05 |

patterns were characterised by three groups: $C_o$ threshold determined (Pattern 1 and 4), $q_s/q_{s,max}$ threshold determined (Pattern 2 and 6), and combined threshold determined (Pattern 3 and 5). Fig. 2B shows schematic lifelines of Pattern 1, 2, and 5 for illustration of the three groups. Since Pattern 1 was $C_o$ threshold determined, its oxygen lifeline started and ended with a maximum $C_o$ of 0.05 mmol/L, and the profile could be characterised using the arc-analysis approach proposed in prior work (Haringa, Tang et al. 2016). The minimum $C_o$ ($C_{o,min}$) and the time scale to reach $C_{o,min}$ were used to determine the DO arc magnitude and arc duration, respectively. For the conditions classified as glucose limiting, the criterion was that the glucose lifelines remained in the Limitation sub-regime range ($0.05 < q_s/q_{s,max} < 0.95$). As shown in Fig. 2C, neither maximum nor minimum $q_s/q_{s,max}$ correlated to the begin or end point; the lifelines usually started at $q_s/q_{s,max} \sim 0.78$ and ended $\sim 0.74$, the minimum $q_s/q_{s,max}$ had a correlation to time scale ($t$), and could drop down to 0.4 when $t > 40$ s. Hence, the lifeline could not be characterised by the arc-analysis and the profile may be more arbitrary.

As $q_s/q_{s,max}$ threshold determined, the glucose lifeline of Pattern 2 could be characterised by the arc-analysis similar to the unlimited oxygen scenario (Haringa, Tang et al. 2018), whereas the oxygen lifeline may have a more arbitrary profile in the oxygen-Sufficient sub-regime range ($C_o > 0.05$ mmol/L). Regarding Pattern 5, which is characterised by combined glucose-oxygen thresholds, the oxygen lifeline started with the minimum $C_o$ of 0.05 mmol/L, and generally had an increasing trend (may not be monotonic) since the trajectory moved from top towards bottom of the bioreactor. In contrast, the glucose lifeline generally had a decreasing trend, and ended with the minimum $q_s/q_{s,max}$ of 0.05. For Pattern 4, 6, and 3, the lifeline characterisations were carried out similar to Pattern 1, 2, and 5, respectively. Moreover, Fig. 2A contains the information of logical sequences for pattern connections. For example, Pattern 1 started from Pattern 3 or 4, and was followed by Pattern 4 or 5. As shown in Fig. 2D, the connecting points (between the end point of Pattern 3 or 4, and the first point of Pattern 1) had a good correlation in $q_s/q_{s,max}$ values. Similar results were obtained in the other pattern connections (data not shown), so any concentration discontinuity in lifelines during pattern switches could be negligible. These different lifeline characteristics in regime-transition patterns and logical pattern sequences were also considered in constructing and connecting lifelines in the SD simulators, which are described in Section 3.2.1 and 3.2.3.

The residence time distributions of the six re-defined regime-transition patterns are shown in Fig. 2E. All these patterns generally had an exponential decay trend, especially when the residence time was over 10 s, similar to the results of the unlimited oxygen scenario in this study (data not shown) and in the previous work (Haringa, Tang et al. 2016, Haringa, Tang et al. 2018). However, considerable differences were

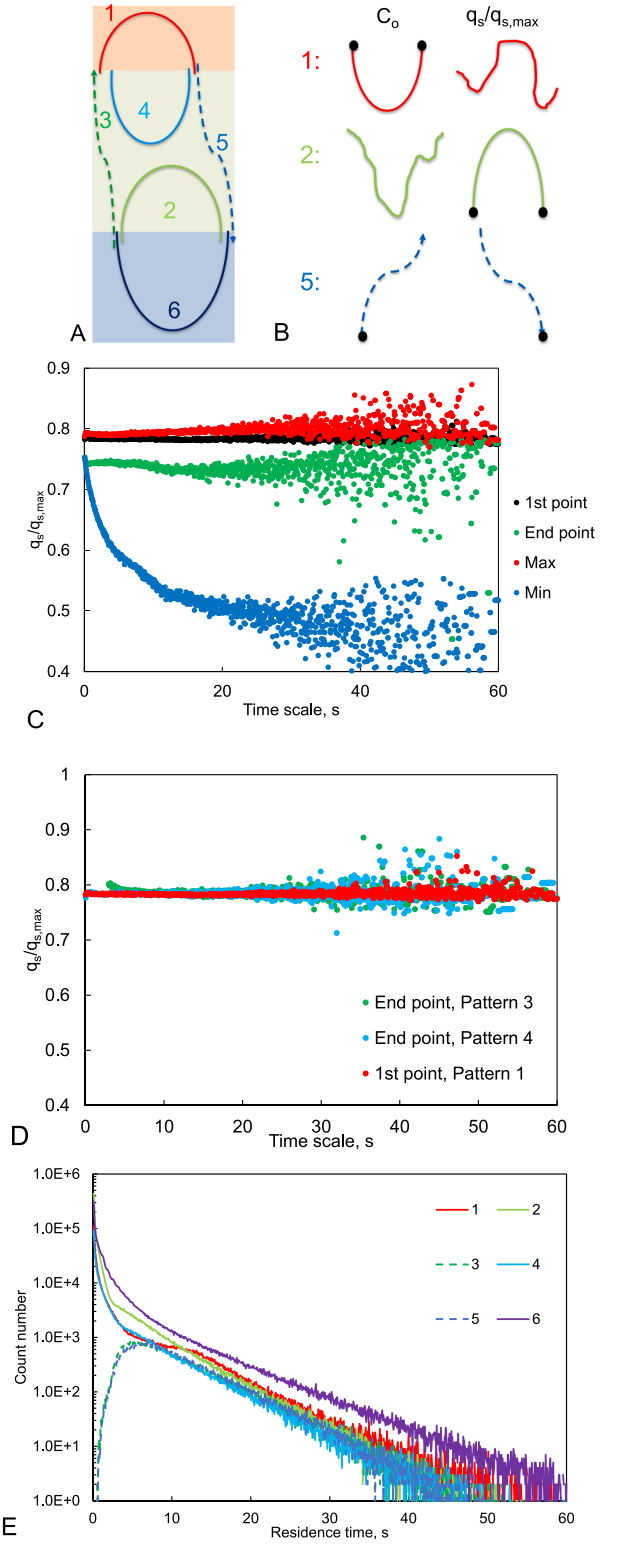


**Fig. 2.** (A) Six new regime-transition patterns obtained in the studied industrial fermentor, distributed with logical connections; (B) schematic glucose uptake ($q_s/q_{s,max}$) and oxygen ($C_o$) lifelines of Pattern 1, 2, and 5 (black dots denote limiting points); (C) $q_s/q_{s,max}$ of the first point, end point, maximum, and minimum in the glucose lifelines of Pattern 1, as a function of time scale; (D) $q_s/q_{s,max}$ of the connecting points (between the end point of Pattern 3 or 4, and the first point of Pattern 1), as a function of time scale; (E) residence time distributions of the six regime-transition patterns.

found in the small timescales. Pattern 3 and 5 had little probability when the residence time was < 5 s. Since the two patterns accounted for the transition between the regimes located in the top (L-) and bottom (S +), minimal time to travel through the whole L + regime was required. Moreover, the other four patterns had different exponential decay rates in small residence time scales. This was similar to the unlimited oxygen scenario (Haringa, Tang et al. 2016), and indicated different circulation loops dominated the biomass motion in each regime. Although with some differences in the decay rate, the overall exponential decay behaviour still indicated a circulation condition in each regime in terms of hydrodynamic behaviour. This indicates that in single-reactor SD mode, variable time intervals can be used to mimic the circulation time distribution in the large-scale vessel, basing the regimes on a consistent metabolic response. Of course, there are still concentration gradients inside these regimes; the glucose/DO distribution is not ideally mixed in the literal sense.

#### 3.1.4. Hypothesised more severe glucose-oxygen gradients, and the impact of oxygen transfer kinetics

The simulation results can be used to further develop the SD framework (from industrial-scale) considering glucose-oxygen limitations. However, the results did not demonstrate a large oxygen-Limited zone in the studied bioreactor. More severe oxygen (DO starvation) conditions have been considered in some lab-scale work (Larsson and Enfors 1985, McIntyre et al., 1999).

To study if such conditions are expected to appear under more intense fermentation conditions, we considered a doubled glucose feed rate (both for the Roels and Tsao & Hanson models), while the other settings remained the same. The results are shown in Table 1. As mentioned in Section 3.1.1, the differences between the two models will not be discussed, and only Tsao & Hanson's data are analysed here. A considerable fraction (33.8%) of the oxygen-Limited regime (only L- as well) was obtained when a double glucose feed rate was applied, which was also included in the following SD design. Moreover, assessing the sensitivity of the mass transfer model, some adjustments in stirring speed, bubble size, and broth rheology were found to considerably affect the estimation of oxygen transfer rate ($k_La$) from gas to liquid (Table S2), which propagated into substantially affecting the oxygen gradients. These hypothetical adjustments were based on reasonable assumptions, and their importance is clear from the CFD simulations as well as from the previous work (Haringa, Tang et al. 2018). Unfortunately, no relevant experimental data is available for the studied bioreactor. Hence, we can only highlight the qualitative relevance here. Future work focusing on experimental quantification of these parameters in industrial-scale facilities would be highly valuable.

### 3.2. Setup and operational design of scale-down simulators, based on the industrial-scale analysis

#### 3.2.1. Representation of predicted industrial-scale metabolic regimes & lifelines

The results in Section 3.1.3 illustrated that the re-definition of the metabolic regimes did not qualitatively change the key lifelines characteristics: frequent and rapid switches between metabolic regimes. As described in Section 2.2, the prior SD approach (Haringa, Tang et al. 2018) still forms a basis for the first variant (SD-A) of the SD simulator design in this study, and was further developed to construct the oxygen-related lifelines. For each regime-transition pattern, the distinct profile characteristics described in Section 3.1.3 were referred to construct the SD glucose and oxygen lifelines. Since glucose and oxygen uptake rates ($q_s$ and $q_o$) were dependent on both $C_s$ and $C_o$ (Equation (1) and (2), their changes would be more complex when $C_s$ and $C_o$ were varying simultaneously. To reduce the complexity of lifeline construction in SD-A, some assumptions (e.g., constant $C_s$ or $C_o$ in specified duration) were considered to minimise the frequency of on–off switches for glucose feed and oxygen supply in each regime-transition pattern. Pattern connections were determined based on the logical pattern sequences, and the connection choice statistically depended on probability of the relevant patterns. As shown in Table 3, the fractions of both the metabolic regimes and the regime-transition patterns predicted in SD-A are quite close to the CFD lifeline data (deviation < 2%), showing that the design has the potential to represent the currently predicted industrial-scale regime characteristics.

#### 3.2.2. Translation to SD experiments: Performance assessment and optimisation

The randomised construction of glucose and oxygen lifelines in SD-A requires highly variable conditions for both glucose feed and oxygen supply, which will be even more difficult to practically impose in an SD simulator than the unlimited oxygen scenario. To solve the SD-A's limitation, an effective translation to practical SD implementation is required. As described in Section 2.2, SD-B was designed based on an experimental SD simulator, which was run to mimic the glucose-oxygen limitations predicted in the studied fermentor (here shows the hypothesised scenario with stronger glucose-oxygen limitations). As a restriction to the design of this SD protocol, the basic experimental setup was mainly referring to some previous studies (Larsson and Enfors 1985, de Jonge et al., 2011, McIntyre et al., 1999). Thus, the glucose-oxygen limitations were represented by the combination of one glucose-famine phase and one DO-starvation phase in a single cycle, whereas the two phases were not overlapping.

The same setup was assumed in SD-B first, to assess the performance of the referred experimental SD simulator. As shown in Table 4, considerable fraction differences were obtained in all metabolic regimes between CFD (the second row) and SD-B (the third row). So this SD experiment seems not able to match the metabolic regime distributions predicted in the industrial-scale bioreactor. To improve the performance, the SD-B setup was further optimised by adjusting the oxygen and feed supply conditions in a single cycle, including flow rate and duration of the DO-supply (aeration) phase, and the glucose feed rate. However, the optimised setup (SD-B, Opt. 1, and Opt. 2 in Table 4) could only have a good agreement in some regimes, while with considerable deviation in the other. Besides, the S- regime was absent in the CFD results, but could still be predicted in SD-B even after the optimisations. So the discrepancy to the industrial-scale data seems intrinsic in SD-B, indicating the limitation of the applied combination of single glucose-famine phase and DO-starvation phase. In addition, the biomass concentration in SD-B (6 g/L) was lower than SD-A (27.5 g/L), leading to slower glucose and DO consumption; the on–off switches for the glucose feed and oxygen supply had a time scale at least in the order of $10^1$ s. Hence, the rapid fluctuations (in $10^0$ s) in the industrial-scale lifelines could not be resolved in SD-B, even with optimisations. Although commonly applied in previous SD studies (Larsson and Enfors 1985, de Jonge et al., 2011, McIntyre et al., 1999, Wang et al., 2018), the setup based on single switch of glucose feast-famine or DO supply-starvation with a relative large time scale and low biomass concentration, was found to have intrinsic limitation to represent the industrial-scale data, and thus needs to be further improved.

**Table 3**
Fractions (%) of metabolic regimes and regime-transition patterns predicted in the studied fermentor (CFD) and SD-A.

| | | CFD, $C_x$ 55 g/L | SD-A, $C_x$ 27.5 g/L |
|---|---|---|---|
| **Metabolic regime** | L- | 14.8 | 13.5 ± 0.3 |
| | L+ | 37.7 | 37.4 ± 0.4 |
| | S+ | 47.5 | 49.1 ± 0.3 |
| **Regime-transition pattern** | 1 | 12.4 | 11.7 ± 0.2 |
| | 2 | 35.8 | 36.4 ± 0.7 |
| | 3 | 1.8 | 1.9 ± 0.02 |
| | 4 | 10.5 | 9.7 ± 0.3 |
| | 5 | 1.8 | 1.9 ± 0.02 |
| | 6 | 37.6 | 38.3 ± 0.7 |

**Table 4**
Metabolic regime fractions predicted in the studied fermentor (CFD), SD-B (including the referred SD experiment and 2 optimised settings, with estimated glucose feed and air supply conditions), and new SD simulator (SD-C).

| | | $C_x$, g/L | Metabolic regime fraction, % | | | | Estimated conditions in a cycle | | |
|---|---|---|---|---|---|---|---|---|---|
| | | | S- | L- | S+ | L+ | Cycle time, s | Glucose feed | Air supply |
| CFD | | 55 | 0 | 33.8 | 8.0 | 58.2 | – | – | – |
| SD-B | Exp. referred | 6 | 13.4 | 12.3 | 31.5 | 42.8 | 360 | 0–36 s ON, 4e-5 mol/s | 84–244 s ON, 2.0 L/min |
| | Opt. 1* | | 5.4 | 34.3 | 23.1 | 39.6 | | 0–36 s ON, 5e-5 mol/s | 72–324 s ON, 2.7 L/min |
| | Opt. 2* | | 21.0 | 17.1 | 8.3 | 53.6 | | 0–36 s ON, 5e-5 mol/s | 72–288 s ON, 3.2 L/min |
| SD-C (new design) | | 20 | 0.1 | 34.8 | 10.4 | 54.7 | 194 | ** | ** |
| | | 10 | 0.9 | 35.6 | 9.3 | 54.3 | | | |
| | | 6 | 1.9 | 34.1 | 8.0 | 56.0 | | | |

*: Optimised (Opt.) glucose feed and air supply conditions, and the other settings were kept the same with the referred SD experiment.
**: Details of the conditions are summarised in Table 5.

### 3.2.3. *Further improvement: A new SD simulator design*

Regarding the limitations of SD-A and SD-B, a new SD simulator (SD-C) was designed in this step. To effectively translate to practical SD experiments, SD-C considered periodic cycles with specified settings for glucose feed and DO supply conditions, instead of the randomised setup in SD-A. To obtain a better match with the fluctuations observed in the CFD data, SD-C also included the time scale, frequency, and logical sequence of the regime-transition patterns missed in SD-B. The basic cycle setup of SD-C is shown in Fig. 3, which is divided into six steps. Each step accounts for one type of regime-transition pattern switches. The mean residence time and probability of the six regime-transition patterns (in Table S3) were used to specify their time scale and switch frequency in the whole cycle. The logical pattern sequences were used to arrange the switch type in each step and the sequence of the six steps. Generally, Step 1 contains a number of transition loops between the connected Pattern 1 and 4, accounting for the frequent switches between the L- and L + regimes observed in the CFD lifeline data. Similarly, Step 4 contains loops between Pattern 2 and 6, accounting for the frequent switches between L + and S +. Step 2 and 3 were set for Pattern 5, and Step 5 and 6 for Pattern 3, which both had large time scales and small probability, and accounted for connecting the two frequent switches in Step 1 and 4.

As shown in Table 4, SD-C ($C_x$ 20 g/L) had a much better agreement in the regime distributions to the CFD data with almost no prediction of S-, compared to all SD-B cases. The small differences (<4%) were acceptable since the setup with periodic cycles and fixed parameters was still an approximation to the statistical characteristics of the CFD data. The predicted SD glucose ($q_s/q_{s,max}$) and oxygen ($C_o$) lifelines (Fig. 4A) demonstrated rapid changes similar to the industrial-scale results. In Step 1 (0 to 92 s), both profiles repeated a steep increase–decrease in a short time (~8 s), to account for the frequent switches between Pattern 1 and 4. Similarly, the frequent switches between Pattern 2 and 6 were reflected in the sharp fluctuations in Step 4 (118 to 176 s).

Generation of SD-C lifelines requires both stable and highly fluctuating conditions for glucose feed and aeration in one cycle. As shown in Table 5 and Fig. 4B, the glucose feed and aeration operations were frequently switched between ON and OFF in some steps. In Step 1, the oxygen supply was periodically turned ON in a short time (4.5 s) with a relatively large amount (over 3 times larger than Step 3), to match the transition between L- and L +. The glucose feed was turned ON at the same time to minimise the generation of S-. In Step 4, pulse glucose feed (0.6 s) was applied and the oxygen supply was kept on to account for the other frequent transition between L + and S +. In the other steps, the glucose feed and oxygen supply operations were not fluctuating but just stable.

Moreover, some recommendations for managing metabolic regime fractions in an SD simulator could be summarised. The glucose-Starvation sub-regimes (S + and S-) were found to be sensitive to both glucose feed and aeration conditions. To minimise the occurrence of S- (not observed in CFD) in the SD experiments, it is suggested that the starting time and time scale of aeration should be closely coupled with the glucose-feed phase, and the glucose feed rate should be at a moderate level (not too high). In order to create more severe glucose-oxygen limitations, increase of S-'s proportion may be required. The presence of S + seems important for system stabilisation, since little or no S + fraction could lead to predict abnormal long-term system performance with large glucose accumulation and insufficient DO (by over consumption). The glucose-Limitation sub-regimes (L + and L-) were found to be more sensitive to changes in the oxygen supply conditions than the glucose feed conditions in the studied range. It could be expected that

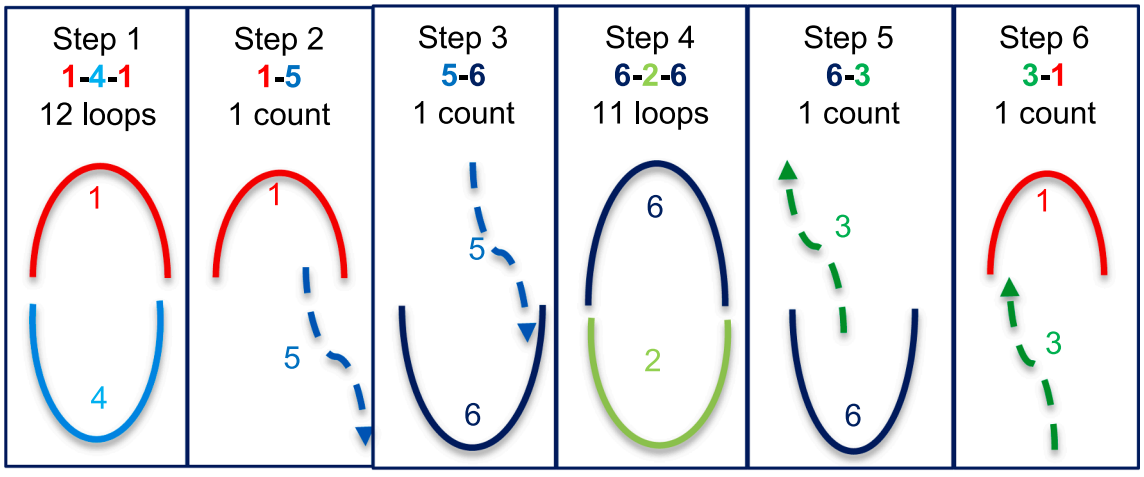


**Fig. 3.** Schematic setup of the new SD simulator (SD-C), six steps included.

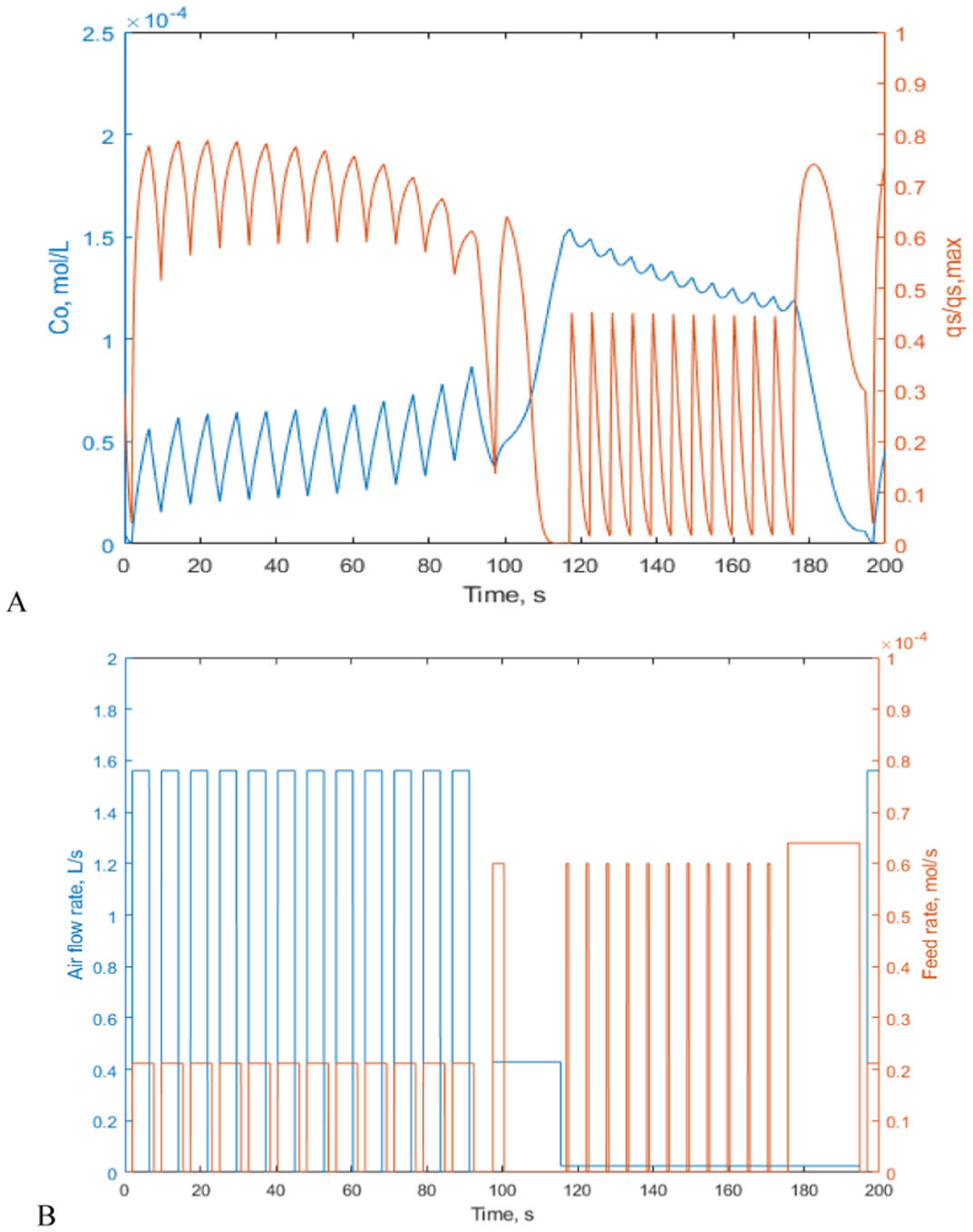


**Fig. 4.** (A) Glucose and DO lifeline profiles, and (B) proposed glucose feed and air supply conditions (based on SD-B configuration), in one cycle (after a fermentation time of 80 h) of SD-C.

**Table 5**
Proposed glucose feed and air supply conditions in the six steps in one cycle of the new SD simulator (SD-C), based on SD-B's configuration.

| | | Step 1 | Step 2 | Step 3 | Step 4 | Step 5 | Step 6 |
|---|---|---|---|---|---|---|---|
| Glucose feed | ON/OFF switch mode (Duration, ×frequency) | 2 s OFF + 5.7 s ON ×12 | All 5 s OFF | 3 s ON + 15 s OFF ×1 | 1.4 s OFF + 0.6 s ON + 3.3 s OFF ×11 | All 1.4 s OFF | All 16.5 s ON |
| | Feed rate in ON, mol/s | 2.1 e-5 | – | 6.0 e-5 | 6.0 e-5 | – | 6.4 e-5 |
| Air supply | ON/OFF switch mode (Duration, ×frequency) | 2 s OFF + 4.5 s ON + 1.2 s OFF ×12 | All 5 s OFF | All 18 s ON | All 58.3 s ON | All 1.4 s ON | All 16.5 s ON |
| | Flow rate in ON, L/s<br>1: Coalescing<br>2: Non-coalescing | 1: 1.55<br>2: 1.1 e-2 | – | 1: 0.43<br>2: 7.7 e-4 | 1: 0.03<br>2: 3.1 e-6 | 1: 0.03<br>2: 3.1 e-6 | 1: 0.03<br>2: 3.1 e-6 |

these recommendations are not only applicable to the current SD setup, but also have the potential to guide further adjustments or hypothetical extensions in SD design.

### 3.2.4. Applicability to experimental SD simulator in practice

It should be noted that the setup in Table 5 was based on SD-B's setup, and the assumptions described in Section 2.2, which should be checked when applying in a practical SD experiment. In theory, the setup can represent the environmental fluctuations required to mimic a full-scale environment, but practically there will be challenges: in a single cycle, there are frequent fluctuations in both feed- and airflow rate. The complexity in the SD setup seems inherent, since the well-mixed SD simulator needs a time sequence of different 'actions' to drive the entire culture to experience the environmental changes that are spatially distributed and experienced by part of the microorganisms in the industrial-scale bioreactor. The approach taken in SD-B ($C_x$ 6 g/L) may be inadequate for SD-C ($C_x$ 20 g/L) because of rheological changes, which may require a higher stirring speed as well as affect mass transfer. A higher stirring speed $N$ requires a lower airflow to achieve the same $k_La$, which may be beneficial concerning the high airflow rates required for the base design of SD-C. Additionally, using pure $O_2$ instead of air or applying measures to reduce the bubble size distribution such as usage of microspargers (Groen et al., 2005) or reducing bubble coalescence may be applied to reduce the airflow rate (in the order of $10^2 \sim 10^4$, also shown in Table 5). Besides, the complex simultaneous operation of devices for glucose feed and aeration should be well programmed and controlled in practice.

Lower biomass concentrations were also applied in SD-C. As shown in Table 4, the scenarios with reduced $C_x$ (6 and 10 g/L) obtained good results in the regime distributions. However, with low $C_x$ it was not possible to realize rapid glucose and DO consumptions. As shown in Fig. 5, the lifelines had much smoother fluctuations; especially in Step 1, some $C_o$ peaks could not cover the threshold value of 0.05 mmol/L. The frequent transitions between L + and L-, and considerable gradients of glucose (maximum $q_s/q_{s,\max}$ up to 0.9) and DO (minimum $C_o < 0.01$ mmol/L) obtained in the CFD model were difficult to be reflected in the low $C_x$ scenarios. Hence, a relatively high $C_x$ seems necessary in SD-C.

As commonly used in previous studies (Sweere et al., 1988b, Wang et al., 2018, George, Larsson et al. 1993, George, Larsson et al. 1998, Haringa, Deshmukh et al. 2017,), the multi-compartment reactor mode was also considered as an alternative scale-down approach. However, the highly fluctuating glucose and oxygen lifelines are more applicable to be constructed in a single bioreactor with frequent temporal condition changes than two bioreactors with frequent spatial variations. Nevertheless, for purpose of completing the exercise, a four-compartment reactor mode was designed, including two compartments of stirred tank reactors (STR), and two compartments of plug flow reactors (PFR), as shown in Fig. S1. However, operating the four-compartment SD simulator may be too challenging in practice. Since frequent changes in glucose and oxygen conditions are still required in the two STRs, the aforementioned challenge in SD-C should also be considered, and thus the four-compartment SD simulator has considerably increased system complexity. And further, pumping broth between compartments introduces possible artefacts, such as shear damage to the cells or oxygen and glucose depletion in the tubing, with increased risks for malfunction and contamination.

Alternative could also be the application of micro-bioreactors, e.g., micro-fluidics, in which the rapid regime transitions are easier to be represented by pulse or sinusoidal feeding of $C_s$ and $C_o$. However, the response of single or a few number of cells cannot fully represent the overall performance of the cell population in industrial-scale system. Thus further work on validation/calibration of SD-C, and implementation of the frequent fluctuations in lifelines in experimental SD simulators would be valuable.

## 4. Conclusions

In this study, glucose-oxygen coupled impacts on metabolism of PEN production in an industrial-scale fermentor were numerically investigated. Based on threshold concentrations of both glucose and oxygen, six metabolic regimes were defined to characterise the coupled impacts. Both Tsao & Hanson and Roels (black-box) models were applied to characterise the glucose-oxygen coupled consumption. The Roels model predicted considerable glucose gradients, whereas less oxygen gradients since a small fraction of the oxygen-Limited regimes was obtained. However, the Tsao & Hanson model predicted distinct regime distributions: with no glucose-Excess regimes and larger oxygen-Limited fraction. These differences make clear that it is important to define and integrate appropriate oxygen-coupled uptake kinetics in the model, preferably using metabolic mechanisms of oxygen action, and implement it in the prior CFD-CRD framework, while the model choice needs to be validated in the future work.

In the Tsao & Hanson model, the glucose gradients ran from top (feed location) to bottom; in contrast, the DO gradients materialised in the opposite direction due to the aeration near the bottom. Compared to the unlimited oxygen scenario, the reduced magnitude of the glucose gradients revealed considerable changes in overall glucose uptake, and the resulting PEN productivity in the studied bioreactor. Regarding the redefined metabolic regimes, the lifeline data showed frequent regime transitions with small characteristic time scales ($10^0 \sim 10^1$ s), indicating

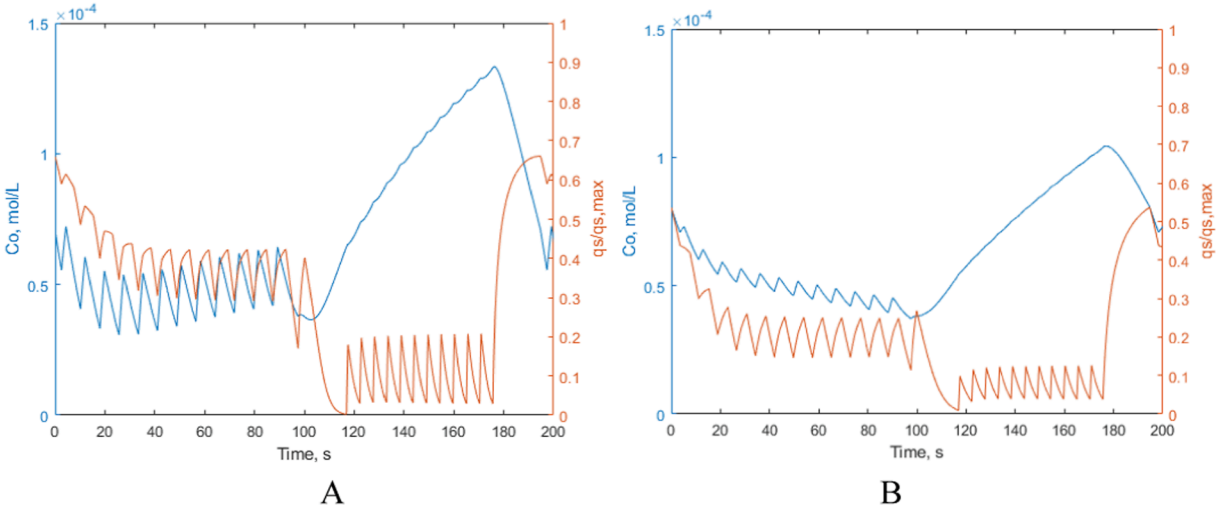


**Fig. 5.** Glucose and DO lifeline profiles in one cycle (after a fermentation time of over 80 h) of SD-C, (A) $C_x$ 10 g/L, (B) $C_x$ 6 g/L.

rapid changes in glucose- and DO-uptake by the microorganisms. It is noted that these rapid fluctuations are usually not covered in experimental studies using SD simulators. Rather, slow cycles in the order of several minutes are applied which is addressing more worst-case performance than a representative scale-down.

Further, the model framework was developed by a hypothetical study (double feed) to create more severe glucose-oxygen gradients, which was not experimentally tested with our PEN case, but may still be highly relevant for general industrial practice. The observed data dependency on modelling the gas–liquid flows, oxygen transfer, and oxygen uptake kinetics, indicated the demand of more accurate insight into the multiphase hydrodynamics and metabolic processes. Some recommendations for managing metabolic regime distributions in SD experiments were also proposed.

Regarding the limitations in the two SD simulators developed based on selected prior SD protocols, a new SD simulator was designed to be both representative to the highly oscillating industrial-scale conditions, and applicable to translate to SD experiments in the lab. The proposed SD setup requires a relatively high biomass concentration, frequent regime switches, and considerable operational fluctuations in glucose feed and oxygen supply, and thus implementation will not be straightforward using commonly used lab-scale STR's and/or PFR's. Rather, we advocate to consider alternative, micro-scale SD simulator set-ups that can accommodate faster changes of the cellular environment, yet capable of maintaining the required amplitude ranges. However, focus should be in reducing time scales of the operational fluctuations (from minutes to 10 s or less) in experimental SD simulators in the future.

## Declaration of Competing Interest

The authors declare that they have no known competing financial interests or personal relationships that could have appeared to influence the work reported in this paper.

## Data availability

The authors do not have permission to share data.

## Acknowledgments

The authors gratefully acknowledge the funding from the ERA CoBioTech/EU H2020 project (grant 722361) "ComRaDes". The authors also thank Dr. Á. Jánoska for the collaborations on the scale-down work. Computational resources are supported by the high-performance computing facilities from Delft University of Technology.

## Appendix A. Supplementary data

Supplementary data to this article can be found online at https://doi.org/10.1016/j.ces.2023.118770.

## References

Clift, R., Grace, J.R., Weber, M.E., 1978. Bubbles, drops, and particles. Academic Press, New York.

Cui, Y.Q., van der Lans, R.G.J.M., Luyben, K.C.A.M., 1996. Local power uptake in gas-liquid systems with single and multiple rushton turbines. Chemical Engineering Science 51 (11), 2631–2636.

de Jonge, L.P., Buijs, N.A.A., ten Pierick, A., Deshmukh, A., Zhao, Z., Kiel, J.A.K.W., Heijnen, J.J., van Gulik, W.M., 2011. Scale-down of penicillin production in Penicillium chrysogenum. Biotechnology Journal 6 (8), 944–958.

Douma, R.D., Verheijen, P.J.T., de Laat, W.T.A.M., Heijnen, J.J., van Gulik, W.M., 2010. Dynamic gene expression regulation model for growth and penicillin production in Penicillium chrysogenum. Biotechnology and Bioengineering 106 (4), 608–618.

George, S., Larsson, G., Enfors, S.O., 1993. A scale-down two-compartment reactor with controlled substrate oscillations: Metabolic response of Saccharomyces cerevisiae. Bioprocess Engineering 9 (6), 249–257.

George, S., Larsson, G., Olsson, K., Enfors, S.O., 1998. Comparison of the Baker's yeast process performance in laboratory and production scale. Bioprocess Engineering 18 (2), 135–142.

Groen, D. J., H. J. Noorman and A. I. Stankiewicz (2005). Improved method for aerobic fermentation intensification. Proceedings of Sustainable (Bio)Chemical Process Technology Incorporating 6th Int. Conf. Process Intensification, BHR Group Limited.

Gunyol, O., Noorman, H.J., Mudde, R.F., 2009. CFD simulations of a large-scale fermenter with muliple impellers. World Congress of Chemical Engineering, University Montreal, 8th.

Hajian, C.S.S., Haringa, C., Noorman, H., Takors, R., 2020. Predicting By-Product Gradients of Baker's Yeast Production at Industrial Scale: A Practical Simulation Approach. Processes 8 (12), 1554.

Haringa, C., Tang, W., Deshmukh, A.T., Xia, J., Reuss, M., Heijnen, J.J., Mudde, R.F., Noorman, H.J., 2016. Euler-Lagrange computational fluid dynamics for (bio)reactor scale down: An analysis of organism lifelines. Engineering in Life Sciences 16 (7), 652–663.

Haringa, C., Deshmukh, A.T., Mudde, R.F., Noorman, H.J., 2017a. Euler-Lagrange analysis towards representative down-scaling of a 22m3 aerobic S. cerevisiae fermentation. Chemical Engineering Science 170, 653–669.

Haringa, C., Noorman, H.J., Mudde, R.F., 2017b. Lagrangian modeling of hydrodynamic–kinetic interactions in (bio)chemical reactors: Practical implementation and setup guidelines. Chemical Engineering Science 157, 159–168.

Haringa, C., Tang, W., Wang, G., Deshmukh, A.T., van Winden, W.A., Chu, J., van Gulik, W.M., Heijnen, J.J., Mudde, R.F., Noorman, H.J., 2018. Computational fluid dynamics simulation of an industrial P. chrysogenum fermentation with a coupled 9-pool metabolic model: Towards rational scale-down and design optimization. Chemical Engineering Science 175, 12–24.

Heins, A.-L., Lencastre Fernandes, R., Gernaey, K.V., Lantz, A.E., 2015. Experimental and in silico investigation of population heterogeneity in continuous Sachharomyces cerevisiae scale-down fermentation in a two-compartment setup. Journal of Chemical Technology & Biotechnology 90 (2), 324–340.

Henriksen, C.M., Nielsen, J., Villadsen, J., 1997. Influence of the Dissolved Oxygen Concentration on the Penicillin Biosynthetic Pathway in Steady-State Cultures of Penicillium chrysogenum. Biotechnology Progress 13 (6), 776–782.

Higbie, R., 1935. The rate of absorption of a pure gas into a still liquid during short periods of exposure. Trans. AIChE 31, 365–389.

Janoska, A., Verheijen, J.J., Tang, W., Lee, Q., Sikkema, B., van Gulik, W.M., 2022. Influence of oxygen concentration on the metabolism of Penicillium chrysogenum. Engineering in Life Sciences n/a(n/a), 1–17.

Khopkar, A.R., Aubin, J., Xuereb, C., Le Sauze, N., Bertrand, J., Ranade, V.V., 2003. Gas−Liquid Flow Generated by a Pitched-Blade Turbine: Particle Image Velocimetry Measurements and Computational Fluid Dynamics Simulations. Industrial & Engineering Chemistry Research 42 (21), 5318–5332.

Kuschel, M., Takors, R., 2020. Simulated oxygen and glucose gradients as a prerequisite for predicting industrial scale performance a priori. Biotechnology and Bioengineering 117 (9), 2760–2770.

Lamont, J.C., Scott, D.S., 1970. An eddy cell model of mass transfer into the surface of a turbulent liquid. AIChE Journal 16 (4), 513–519.

Lapin, A., Müller, D., Reuss, M., 2004. Dynamic Behavior of Microbial Populations in Stirred Bioreactors Simulated with Euler−Lagrange Methods: Traveling along the Lifelines of Single Cells. Industrial & Engineering Chemistry Research 43 (16), 4647–4656.

Lapin, A., Schmid, J., Reuss, M., 2006. Modeling the dynamics of E. coli populations in the three-dimensional turbulent field of a stirred-tank bioreactor—A structured–segregated approach. Chemical Engineering Science 61 (14), 4783–4797.

Larsson, G., Enfors, S.-O., 1985. Influence of oxygen starvation on the respiratory capacity of Penicillium chrysogenum. Applied Microbiology and Biotechnology 21 (3), 228–233.

Larsson, G., Enfors, S.O., 1988. Studies of insufficient mixing in bioreactors: Effects of limiting oxygen concentrations and short term oxygen starvation on Penicillium chrysogenum. Bioprocess Engineering 3 (3), 123–127.

Larsson, G., Törnkvist, M., Wernersson, E.S., Trägårdh, C., Noorman, H., Enfors, S.O., 1996. Substrate gradients in bioreactors: origin and consequences. Bioprocess Engineering 14 (6), 281–289.

Leonard, B. P. and S. Mokhtari (1990). ULTRA-SHARP nonoscillatory convection schemes for high-speed steady multidimensional flow. United States, NASA Lewis Research Center. **NASA-TM-102568 (ICOMP-90-12)**.

Manfredini, R., Cavallera, V., Marini, L., Donati, G., 1983. Mixing and oxygen transfer in conventional stirred fermentors. Biotechnology and Bioengineering 25 (12), 3115–3131.

McIntyre, M., Berry, D.R., McNeil, B., 1999. Response of Penicillium chrysogenum to oxygen starvation in glucose- and nitrogen-limited chemostat cultures. Enzyme and Microbial Technology 25 (3), 447–454.

Neubauer, P., Junne, S., 2010. Scale-down simulators for metabolic analysis of large-scale bioprocesses. Current Opinion in Biotechnology 21 (1), 114–121.

Noorman, H., 2011. An industrial perspective on bioreactor scale-down: What we can learn from combined large-scale bioprocess and model fluid studies. Biotechnology Journal 6 (8), 934–943.

Noorman, H., W. Van Winden, J. Heijnen and R. Van Der Lans (2018). "Intensified fermentation processes and equipment.".

Roels, J. A. (1983). Energetics and kinetics in biotechnology, Elsevier biomedical press.

Shih, T.-H., Liou, W.W., Shabbir, A., Yang, Z., Zhu, J., 1995. A new k-∈ eddy viscosity model for high reynolds number turbulent flows. Computers & Fluids 24 (3), 227–238.

Steel, R., Maxon, W.D., 1966. Dissolved oxygen measurements in pilot- and production-scale novobiocin fermentations. Biotechnology and Bioengineering 8 (1), 97–108.

Sweere, A.P.J., Janse, L., Luyben, K.C.A.M., Kossen, N.W.F., 1988a. Experimental simulation of oxygen profiles and their influence on baker's yeast production: II. Two-fermentor system. Biotechnology and Bioengineering 31 (6), 579–586.

Sweere, A.P.J., Matla, Y.A., Zandvliet, J., Luyben, K.C.A.M., Kossen, N.W.F., 1988b. Experimental simulation of glucose fluctuations. Applied Microbiology and Biotechnology 28 (2), 109–115.

Sweere, A.P.J., Mesters, J.R., Janse, L., Luyben, K.C.A.M., Kossen, N.W.F., 1988c. Experimental simulation of oxygen profiles and their influence on baker's yeast production: I. One-fermentor system. Biotechnology and Bioengineering 31 (6), 567–578.

Tang, W., Deshmukh, A.T., Haringa, C., Wang, G., van Gulik, W., van Winden, W., Reuss, M., Heijnen, J.J., Xia, J., Chu, J., Noorman, H.J., 2017. A 9-pool metabolic structured kinetic model describing days to seconds dynamics of growth and product formation by Penicillium chrysogenum. Biotechnology and Bioengineering 114 (8), 1733–1743.

Tsao, G.T., Hanson, T.P., 1975. Extended Monod equation for batch cultures with multiple exponential phases. Biotechnology and Bioengineering 17 (11), 1591–1598.

Van't Riet, K., 1979. Review of measuring methods and results in nonviscous gas-liquid mass transfer in stirred vessels. Industrial & Engineering Chemistry Process Design and Development 18 (3), 357–364.

Vardar, F., Lilly, M.D., 1982. Effect of cycling dissolved oxygen concentrations on product formation in penicillin fermentations. European journal of applied microbiology and biotechnology 14 (4), 203–211.

Wang, G., Chu, J., Noorman, H., Xia, J., Tang, W., Zhuang, Y., Zhang, S., 2014. Prelude to rational scale-up of penicillin production: a scale-down study. Applied Microbiology and Biotechnology 98 (6), 2359–2369.

Wang, G., Tang, W., Xia, J., Chu, J., Noorman, H., van Gulik, W.M., 2015. Integration of microbial kinetics and fluid dynamics toward model-driven scale-up of industrial bioprocesses. Engineering in Life Sciences 15 (1), 20–29.

Wang, G., Zhao, J., Haringa, C., Tang, W., Xia, J., Chu, J., Zhuang, Y., Zhang, S., Deshmukh, A.T., van Gulik, W., Heijnen, J.J., Noorman, H.J., 2018. Comparative performance of different scale-down simulators of substrate gradients in Penicillium chrysogenum cultures: the need of a biological systems response analysis. Microbial Biotechnology 11 (3), 486–497.